ACS Energy LETTERS

http://pubs.acs.org/journal/aelccp

Solvent Molecule Design Enables Excellent Charge Transfer Kinetics for a Magnesium Metal Anode

Fei Wang, Haiming Hua, Dongzheng Wu, Jialin Li, Yaoqi Xu, Xianzhen Nie, Yichao Zhuang, Jing Zeng,* and Jinbao Zhao*

Cite This: *ACS Energy Lett.* 2023, 8, 780−789

Read Online

ACCESS | Metrics & More | Article Recommendations | Supporting Information

ABSTRACT: **Lacking of suitable electrolytes is a fatal obstacle for the development of rechargeable magnesium batteries (RMBs). Herein, according to the design of a series of solvent molecules, we find 3-methoxypropylamine possesses a middle coordination ability that can be used as an effective solvent and realize a reversible Mg anode with traditional Mg salts. Mechanism study indicates, attributed to its unique solvated structure, energy barriers in both the charge transfer process and desolvation process are extremely low, thus leading to the fast charge transfer kinetics. The relationship between solvated structures and performances is precisely revealed for the first time in RMBs. Additionally, electrolytes with amine solvents possess outstanding water-resistant properties owing to strong hydrogen bonds between amine groups and water. This work proposes a universal design principle of solvent molecules for RMBs, inspiring a new thinking of developing advanced electrolytes in the view of solvents.**

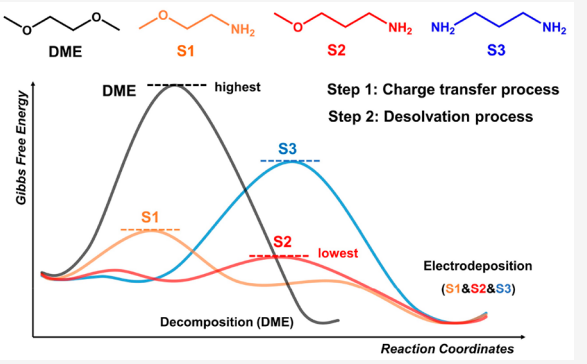

Lithium-ion batteries have ushered in a revolution ranging from portable electronic equipment to electric vehicles.[1−4] However, their further large-scale application is still hampered by unsatisfied energy density, safety anxiety, and high cost.[5−9] Therefore, exploration of an alternative battery system has attracted much attention recently.[10−14] Among numerous candidates, rechargeable magnesium batteries (RMBs) are expected to become a potential next-generation energy storage system because of their following advantages, such as high volumetric energy density (3833 mAh cm^{-3}),[15−19] the intrinsic property of a low tendency to dendritic formation, and low reactivity with air and moisture.[20−24] In addition, abundant Mg resources in the earth's crust can relieve the concern about the limitation of metal resources effectively.[25−30] Unfortunately, the bivalent nature causes an unwished high charge density for the Mg^{2+} ion, leading to a strong electrostatic interaction and an extremely sluggish Mg^{2+} ion diffusion kinetic in most materials.[31−39] For this reason, in sharp contrast with Li metal, the solid-electrolyte interphase (SEI) on Mg metal anode is not Mg^{2+}-conducting and is even called a passivation layer for RMBs, showing large overpotentials and irreversible Mg plating/stripping behaviors. Typically, Mg metal is passivated in traditional electrolytes which contain conventional polar solvents (such as ethylene carbonate and acetonitrile) and simple Mg^{2+} salts (such as $Mg(TFSI)_2$ and $Mg(ClO_4)_2$), leading to incompatibility with a Mg metal anode, even though these traditional electrolytes show attractive advantages of commercial accessibility and low cost.[15,40] This fatal obstacle brings huge challenges to the research of RMBs and hinders the development of RMBs seriously.

Owing to lacking effective SEI layers, an important current electrolyte research consensus is to develop reductively stable electrolytes which are less liable to react with the Mg electrode in thermodynamics, such as reduction-resistant salts dissolved in ether-based solvent, and thus the exposed fresh Mg surface can support reversible Mg plating/stripping.[41−43] Although considerable advances have been accomplished in recent two decades,[44−50] these new-type electrolytes still suffer from many

Received: November 7, 2022
Accepted: December 19, 2022

https://doi.org/10.1021/acsenergylett.2c02525
ACS Energy Lett. 2023, 8, 780−789

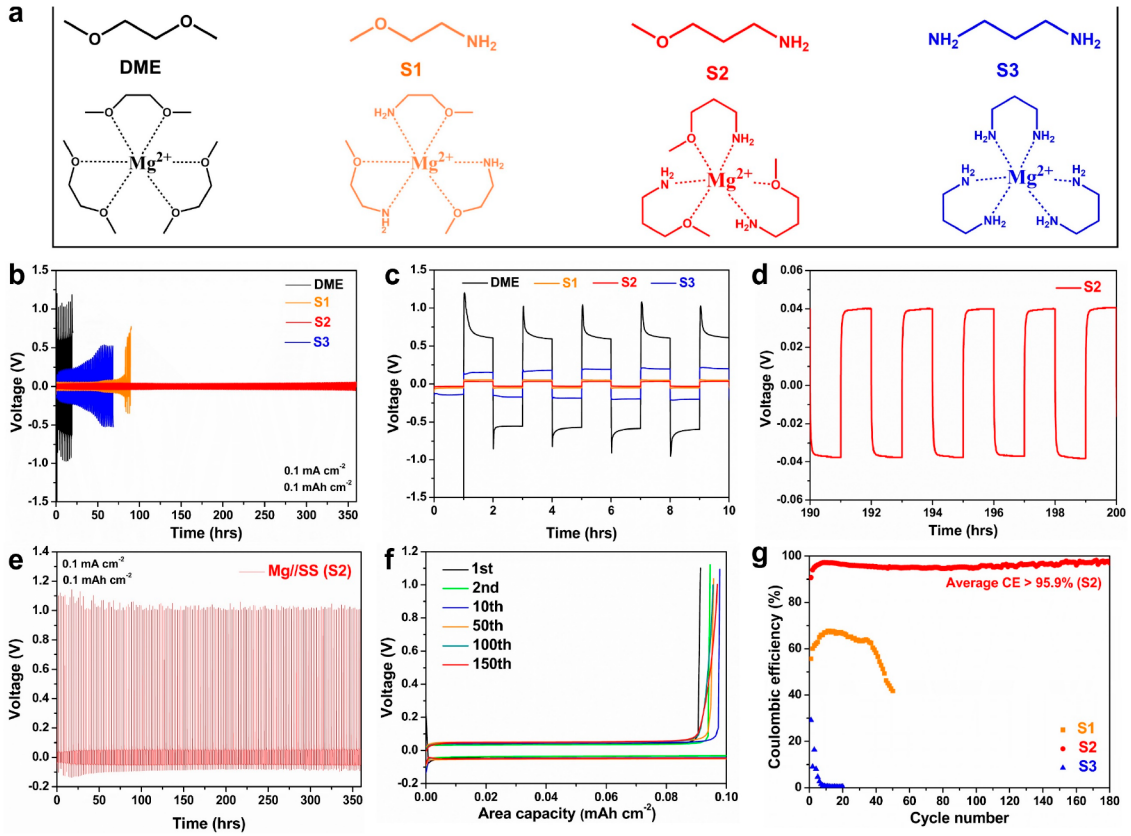

Figure 1. (a) The structures of designed solvent molecules and their corresponding speculated solvated structures with Mg^{2+} ions. (b–d) Galvanostatic cycling performances of DME, S1, S2, and S3 solvents with 0.1 M $Mg(TFSI)_2$ in Mg//Mg symmetric cells at 0.1 mA cm^{-2} for 0.1 mAh cm^{-2}. (e,f) Voltage profiles of S2 solvent with 0.1 M $Mg(TFSI)_2$ in a Mg//SS asymmetric cell at 0.1 mA cm^{-2} for 0.1 mAh cm^{-2}. (g) Comparison of the CEs of S1, S2, and S3 solvents with 0.1 M $Mg(TFSI)_2$ in Mg//SS asymmetric cells at 0.1 mA cm^{-2} for 0.1 mAh cm^{-2}.

intractable problems, such as a complex synthesis process, high cost, and Cl^- corrosion. Especially, they nearly all have the disadvantage of the high sensitivity to water content, which could be not suitable for practical commercial application. Hence, under the troublesome research status of electrolytes in RMBs nowadays, it is urgently needed to design the electrolyte system in a new view of dynamics. Until recently, the interfacial kinetics behavior is demonstrated to be highly influenced by Mg^{2+}solvated structures, showing great differences in electrochemical performances. For example, Wang et al. reported the methoxyethyl-amine additives enable highly reversible Mg anodes via solvation sheath reorganization, and this reorganization can bypass the unfavorable desolvation process as well as reduce the overpotential and parasitic reactions.[S1] This remarkable work is a milestone in RMBs and shows the feasibility of promoting interfacial kinetics to achieve high-performance Mg batteries. Besides, Yang and co-workers proposed the trimethyl phosphate (TMP) molecule to compete with 1,2-dimethoxyethane (DME) and replace one of the three bound DME molecules for the coordination with Mg^{2+} because of the electron-rich phosphorus–oxygen bond.[S2] This rearranged solvation sheath can soften the structure deformation of bound DME, leading to a low polarization and a superior cycling performance. However, the relationship between solvated structures and interfacial kinetics processes still lacks an in-depth investigation, and universal design rules of additive or solvent molecules are not revealed.

Herein, according to the structure of the DME molecule, we elaborately design a series of solvent molecules to regulate the Mg^{2+} solvated structures and discover the 3-methoxypropylamine can be selected as a highly effective solvent with excellent electrochemical performances of lowest overpotential and highest Coulombic efficiency (CE) in designed solvents, exhibiting reversible Mg plating/stripping behaviors in conventional Mg salts. To further understand the relationship between solvated structures and performances, we comprehensively examine the influences of interface electrochemistry and propose a theoretical model in which the Marcus electron transfer process is in series with the desolvation process, as these processes play a key role in the reduction of Mg. Attributed to its unique solvated structure, the 3-methoxypropylamine solvent molecule possesses low energy barriers in both processes, leading to excellent charge transfer kinetics and superior anode electrochemical performances. The important interface electrochemical reaction mechanism is proposed in RMBs for the first time. In addition, the 3-methoxypropylamine solvent shows an outstanding water-resistant property even with the addition of over 10 000 ppm of H_2O in the electrolyte, which is attributed to the strong hydrogen bond interaction between amine groups and water, leading to the remained Mg^{2+} solvated structure and nearly no active H_2O molecules in the electrolyte. This interesting phenomenon can vastly inspire a new thinking about improving the electrolyte stability to water by the strong interaction between solvent and water.

The commercial DME, which is widely used as a common solvent in RMBs, is chosen as the design prototype of solvent molecule. Its solvated structure ($Mg(DME)_3^{2+}$) is greatly

https://doi.org/10.1021/acsenergylett.2c02525
ACS Energy Lett. 2023, 8, 780–789

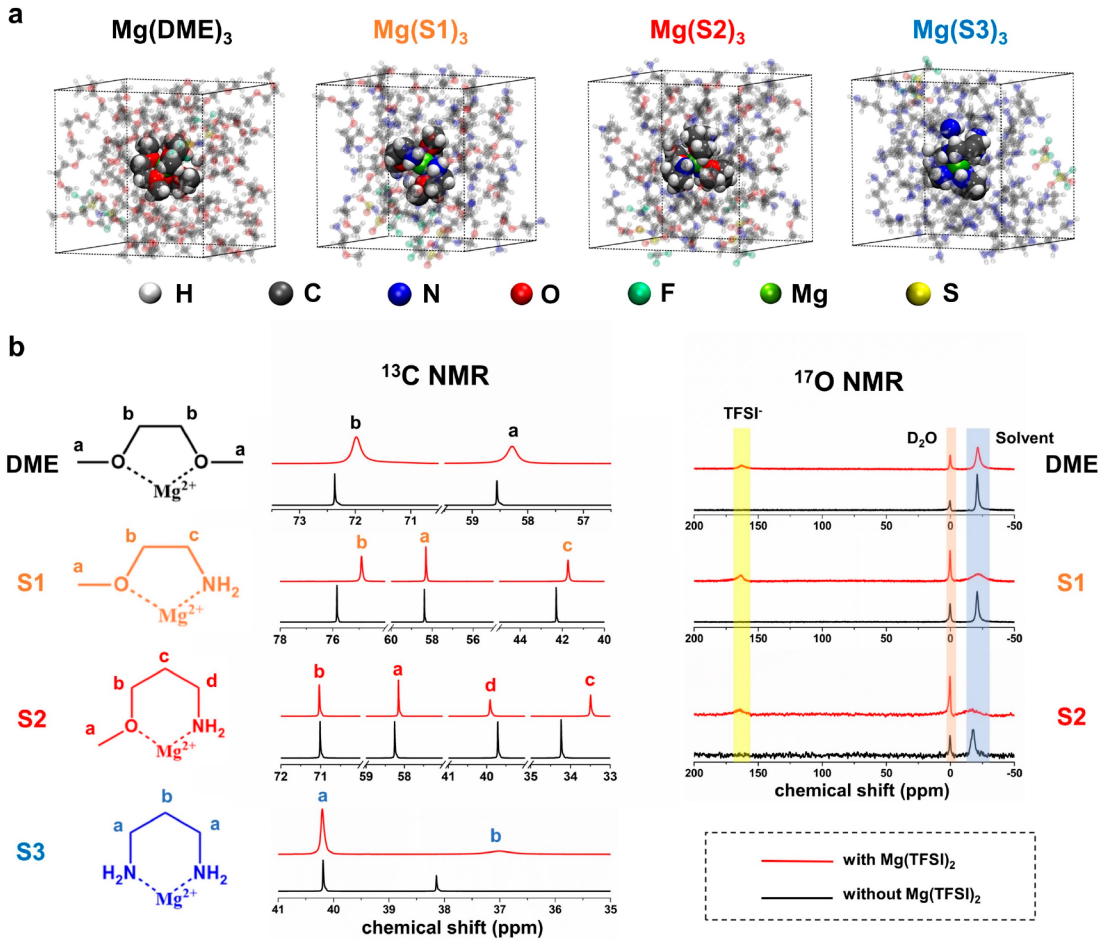

Figure 2. (a) Snapshots of the AIMD simulation boxes of DME, S1, S2, and S3 solvents with $Mg(TFSI)_2$ salt. (b) ^{13}C NMR and ^{17}O NMR spectra of DME, S1, S2, and S3 solvents with and without $Mg(TFSI)_2$ salt.

determined by the coordination atoms (double oxygen atoms) and carbon chain length between coordination atoms. According to this concept, we elaborately regulate the coordination atoms as well as carbon chain length to change coordination structures between solvents and Mg^{2+} ions and propose three solvent molecules: 2-methoxyethylamine, 3-methoxypropylamine, and 1,3-propanediamine (denoted as S1, S2, and S3, respectively). The structures of these solvent molecules and speculated solvated structures are shown in Figure 1a. $Mg(TFSI)_2$ salts (0.1 M) are dissolved into DME, S1, S2, and S3 solvents to form corresponding electrolytes for electrochemical tests, and their ionic conductivities as well as viscosities are shown in Table S1.

The Mg anode plating/stripping behaviors are investigated in Mg//Mg symmetric cells at 0.1 mA cm^{-2} for 0.1 mAh cm^{-2}. As shown in Figures 1b–d and S1a–e, the overpotentials are all reduced in S1, S2, and S3 solvents compared to DME, and especially for S2 solvent, the lowest overpotential is shown below 0.05 V, and an outstanding long-term cycling performance is shown for over 350 h. The CE as an important evaluation criterion to the reversibility of a Mg metal anode is also investigated in Mg//stainless steel (SS) asymmetric cells at 0.1 mA cm^{-2} for 0.1 mAh cm^{-2} (Figures 1e–g and S2a–d). The electrochemical performance of DME in a Mg//SS asymmetric cell is not shown because there is no Mg stripping at the cutoff charge voltage of 1.0 V vs Mg^{2+}/Mg. The average CEs increase from 0.0% in DME to over 95.9% in S2 solvent with the reduction of overpotentials in Mg//Mg symmetric cells, indicating the gradually improved anode reversibility in designed solvent molecules. It is worth emphasizing that this method of just adjusting solvent (replace DME with S2) to realize a reversible Mg metal anode with a low overpotential and high CE is first reported in RMBs, and this method is extremely facile and low cost and avoids the complex synthesis process. Galvanostatic electrochemical tests at a higher current density of 1.0 mA cm^{-2} also show similar results (Figures S3a–d and S4a–d), demonstrating the superior cycling stability with low polarization and improved CEs of designed solvents in different current densities. More kinetics information on Mg plating/stripping is acquired by cyclic voltammetry (CV) and electrochemical impedance spectroscopy (EIS) measurements with a three-electrode system (Figures S5a–d and S6a,b). In addition, electrochemical tests of rate performance as well as high current density and characterization of surface morphology are carried out as well (Figures S7a–d, S8a–d, S9, and S10a–f). These above results unequivocally demonstrate the reversibility of a Mg metal anode, and the Mg stripping/plating kinetics in proposed solvents is remarkably superior to that in DME solvent, especially in S2 solvent.

The surface components of cycled Mg in four electrolytes are measured by X-ray photoelectron spectroscopy (XPS) (Figure S11a). Compared with the DME, the electrolyte decomposition species obviously reduce in S1 and S2, such as −C−F (C 1s), Mg−N (N 1s), Mg−O (O 1s), $-CF_3/CF_2$ (F

https://doi.org/10.1021/acsenergylett.2c02525
ACS Energy Lett. 2023, 8, 780−789

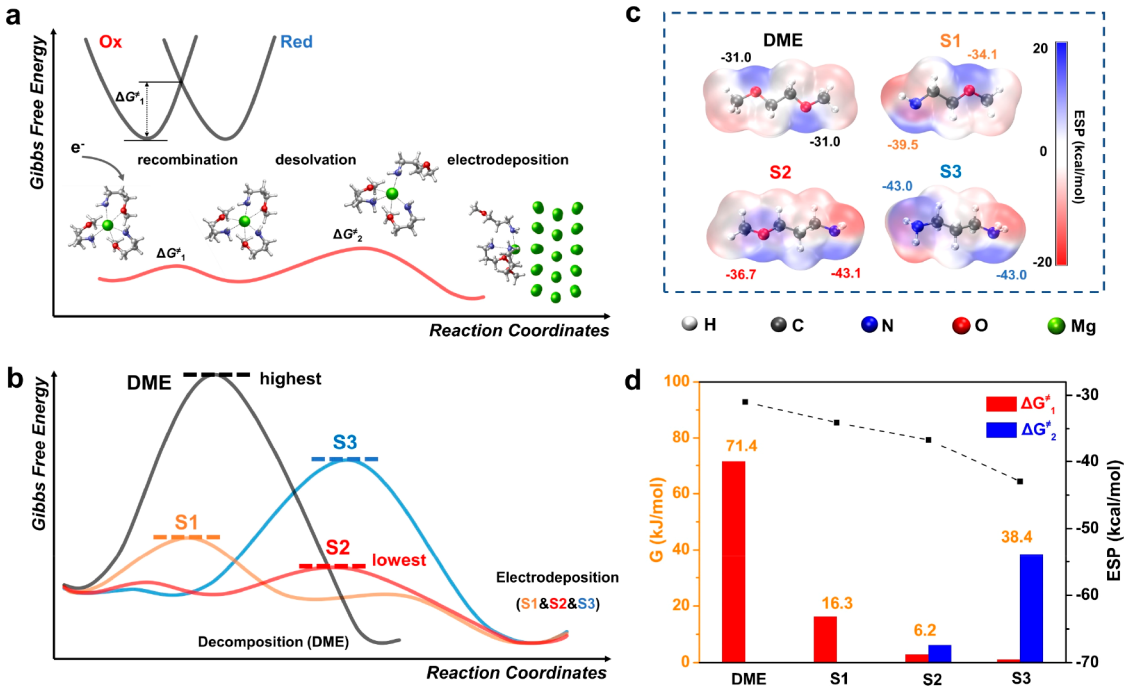

Figure 3. (a) Schematic illustration of the interface electrochemical reaction process in S2 solvent (Marcus charge transfer process and desolvation process). (b) Gibbs activation free energy in the interface electrochemical reaction process for DME, S1, S2, and S3 solvents. (c) The distribution of ESP in DME, S1, S2, and S3 solvents. (d) The relationship between Gibbs activation free energy and ESP in DME, S1, S2, and S3 solvents.

1s), and $-S_x^{2-}$ (S 2p), indicating decomposition of solvent and the $TFSI^-$ anion is greatly suppressed by reducing the overpotential. For S3 solvent, although some decomposition species also reduce according to XPS results, the thickness of the passivation layer formed in S3 is higher (Figure S11b). We speculate this result could be caused by other unknown parasitic reactions in S3 electrolyte, which need further investigations.

Mg^{2+} solvated structures are closely related to different solvents molecules, and it is crucial to understand the influences of different solvated structures in the interface electrochemical reaction. Solvated structures of DME, S1, S2, and S3 solvents are confirmed by the ab initio molecular dynamics (AIMD) simulation and nuclear magnetic resonance (NMR) spectrum. As shown in Figures 2a and S12a−d, the results of simulation and radial distribution functions (RDFs) are as follows: The coordination number of O atoms in DME solvent is six; the coordination numbers of O atoms and N atoms in S1 and S2 solvents are both three, respectively; the coordination number of N atoms in S3 solvent is six. Thus, according to the simulation results, three solvent molecules are coordinated with one Mg^{2+} ion to form chelate solvated structures, which are in perfect agreement with the speculation in Figure 1a. The results of ^{13}C and ^{17}O NMR spectra are shown in Figure 2b. In ^{13}C NMR spectra, obvious position and width changes of characteristic peaks are observed between pure solvents without $Mg(TFSI)_2$ and electrolytes with $Mg(TFSI)_2$. Due to different electronic effects of solvents as well as different ring strains of solvated structures, the size and direction of changes are not exactly regular. In the six-membered coordination structures for S2 and S3 solvents, the middle C atoms (marked "c" in the S2 molecule and "b" in the S3 molecule) show larger changes in chemical shifts compared with other marked C atoms, which could be attributed to the great difference of chemical environment for middle C atoms due to ring tension after coordination. In ^{17}O NMR spectra in which D_2O is used as the capillary internal standard,[53] the characteristic peaks of solvents for DME, S1, and S2 become wider and lower, which indicate the chemical environment of O atoms is changed, further demonstrating O atoms of solvent molecules are coordinated with Mg^{2+} ions in solvated structures.[54] Owing to the stronger coordination ability of the N atom compared to the O atom (Figure 3c, as described later), N atoms are more likely to interact with the Mg^{2+} ion to be involved in the formation of solvated structures. As a consequence, the results of NMR and AIMD simulation indicate that the presumed solvated structures in Figure 1a are the majority structures of Mg^{2+} ions in each electrolyte.

To further understand the in-depth reasons why the overpotentials in S1, S2, and S3 (especially in S2) are much lower than that in DME during Mg plating/stripping process, we investigate the energy barriers of each deposition step in the interface electrochemical reaction process by theoretical calculation of quantum chemistry. Generally, the deposition process of metal contains two main processes: The first process is that solvated clusters receive electrons as well as remove coordinated solvents and subsequently attach to surface of a deposition substrate to form adatoms. The second process is the diffusion of adatoms in the surface of the deposition substrate. As for Mg metal, first, the formation energy barrier of adatoms is higher than its surface diffusion energy barrier under not too high current density.[55] Second, the surface diffusion of Mg mainly depends on the properties of metallic Mg itself (metal bonds and crystal lattice). And thus, we focus on the first process, which plays the most important role in Mg deposition reaction with different electrolytes.

For the first process, it can be further divided into two more elementary processes, namely, a charge transfer process and

https://doi.org/10.1021/acsenergylett.2c02525
ACS Energy Lett. 2023, 8, 780−789

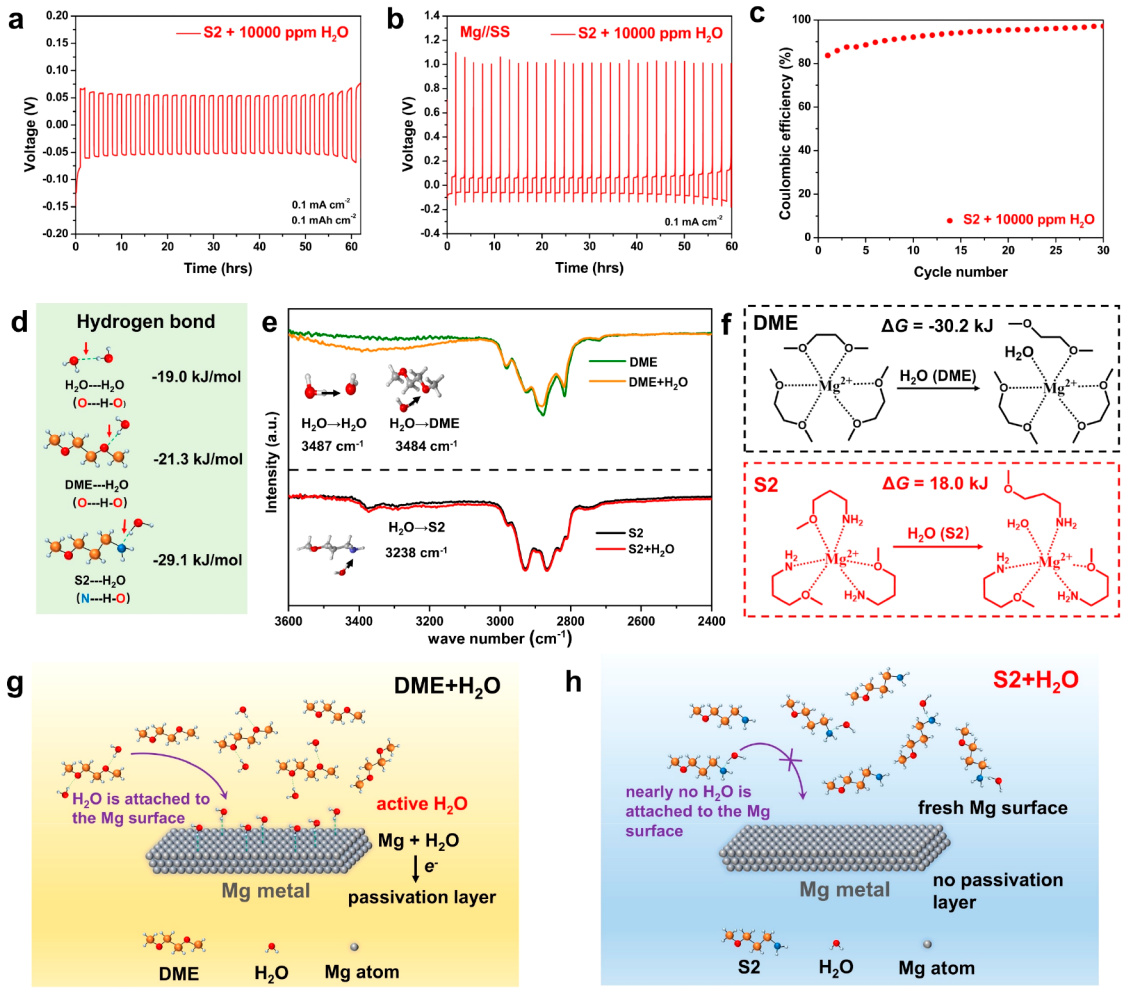

Figure 4. (a) Galvanostatic cycling performance of S2 solvent with addition of 10 000 ppm of H_2O in a Mg//Mg symmetric cell at 0.1 mA cm^{-2} for 0.1 mAh cm^{-2}. (b) Voltage profile and (c) CE of S2 solvent with addition of 10 000 ppm of H_2O in a Mg//SS asymmetric cell at 0.1 mA cm^{-2} for 0.1 mAh cm^{-2}. (d) Bond energies of hydrogen bonds for H_2O to H_2O, DME to H_2O, and S2 to H_2O. (e) FT-IR spectra of 0.1 M $Mg(TFSI)_2$ in DME and S2 solvents (with and without H_2O). (f) Free energies of the entry of water molecules into the first solvated layer of Mg^{2+} ion in DME and S2 solvents. (g) Schematic illustration of the anode passivation mechanism in DME solvent with addition of H_2O. (h) Schematic illustration of the anode protection mechanism in S2 solvent with addition of H_2O.

desolvation process. The energy barrier of the charge transfer process can be analyzed by Marcus theory (Figure S13),[56,57] which is a theoretical model for an electron transfer reaction from the view of kinetics and has achieved great success in the interpretation and prediction of a large number of electrochemical reactions. And the energy barrier of desolvation process can be obtained by the value difference of energy between the solvated structure and desolvated structure. The Gibbs free energy curve of the formation process of an adatom in S2 is shown in Figure 3a. First, a solvated Mg^{2+} ion cluster undergoes the solvation sheath reorganization process (bond length of coordination bonds and solvent conformation are changed), along with an electron transition between two same energy levels at the transition state. The Gibbs activation free energy of the first elementary process is defined as $\Delta G\ddagger_1$, which is relevant to the structure difference of the stable state before and after the electron transition (The $\Delta G\ddagger_1$ increases with difference of structure at two stable states). Subsequently, the solvated Mg cation cluster dissociates one of the coordination O atoms, and then, this Mg cation cluster, which exposes a lone electron, attaches to the surface of a Mg substrate to form an adatom. The Gibbs activation free energy of the second elementary process is defined as $\Delta G\ddagger_2$. The Gibbs free energy curves of the adatom formation process in four electrolytes are shown in Figure 3b, and the structures of key intermediates in four electrolytes are shown in Figure S14a−k as well. The charge transfer process and desolvation process for S1 and S3 are similar to that for S2 (as mentioned above), and the only difference is that for S1 solvent, after the electron transition in the Marcus charge transfer process, the solvated Mg cation cluster has dissociated one of the coordination O atoms spontaneously (Figure S14d), resulting in a very low value for $\Delta G\ddagger_2$ (nearly 0 kJ/mol). As for DME solvent, its electrochemical behavior shows distinct differences. After the electron transition of the solvated Mg^{2+} ion cluster, the C−O bond of the DME molecule has been lengthened and weakened significantly (Figure S14b). Although it may still undergo subsequent desolvation reaction and be reduced to metallic Mg, the higher reduction overpotential (significantly higher $\Delta G\ddagger_1$) and weakened C−O bond indicate that the DME molecule is more likely to decompose through a C−O bond breaking reaction. The situation is consistent with the results of Filhol's group and Yang's group that the Mg deposition reaction could compete with electrolyte decom-

https://doi.org/10.1021/acsenergylett.2c02525
ACS Energy Lett. 2023, 8, 780−789

position in the $Mg(TFSI)_2$/DME electrolyte, leading to decomposition products within the deposition layer.[52,58,59] From overall situation, the apparent activation free energy ($\Delta G‡$) of the Mg electrodeposition process depends on the larger one between $\Delta G‡_1$ and $\Delta G‡_2$. And ranked from largest to smallest, the order of $\Delta G‡$ in four electrolytes is DME (71.4 kJ/mol), S3 (38.4 kJ/mol), S1 (16.3 kJ/mol), and S2 (6.2 kJ/mol), which is greatly consistent with the overpotentials in Mg//Mg symmetric cells (The detailed values of $\Delta G‡_1$ and $\Delta G‡_2$ for four solvents are shown in Table S2).

To further investigate the relationship between $\Delta G‡$ and the solvent structure, the distribution of electrostatic potential (ESP) for the four solvent molecules is obtained by quantitative analysis of the molecular surface using Multiwfn software.[60,61] The ESP is defined as the amount of work energy needed to move a unit of electric charge from infinity to a point on the molecular surface.[62] It could reflect the binding ability of a molecule to the Mg^{2+} ion, as the electrostatic interaction plays a decisive role in the coordination bond of Mg^{2+} ions. A more negative ESP value means a stronger binding trend to the Mg^{2+} ion. The color maps and extreme points of ESP are shown in Figure 3c. Among these molecules, the areas near the N atom and O atom show blue color (negative), which is associated with the lone pair electrons of them. The coordination abilities of solvents gradually increase in the order of DME, S1, S2, and S3. And for the solvents which both contain an O atom and N atom (S1 and S2 solvents), the values of ESP for a N atom are lower compared to an O atom, indicating the coordination ability of a N atom is observably stronger than that of an O atom. To in-depth analyze how the ESP affects $\Delta G‡_1$ and $\Delta G‡_2$, the values of ESP, $\Delta G‡_1$, and $\Delta G‡_2$ of four solvents are summarized and all shown in Figure 3d for comprehensive comparison and analysis. In the order of DME, S1, S2, and S3 solvents, as the values of ESP go down (the dotted line in Figure 3d), $\Delta G‡_1$ decreases gradually as well, while $\Delta G‡_2$ increases gradually, and the $\Delta G‡$ shows the lowest point in S2 solvent as expected. These analysis results demonstrate that for the solvents with stronger coordination ability, the $\Delta G‡_1$ is lower because the structure difference of the stable state before and after an electron transition is small due to the strong coordination effect. However, $\Delta G‡_2$ becomes higher because of the strong coordination effect between the solvent and Mg^{2+} ion. Consequently, the changes of $\Delta G‡_1$ and $\Delta G‡_2$ are antagonistic, and designing the solvent molecule with a middle coordination ability (such as S2 solvent) is a key to enable excellent charge transfer kinetics for a Mg metal anode. Based on the theoretical calculation results and detailed data analysis above, the important interface electrochemical reaction mechanism about the relationship between performance and solvated structures is revealed for the first time in RMBs, which can provide new theory guidance for the design of solvent structure in the future.

The sensitivity to water of an electrolyte is a significant assessment criterion of the possibility of practical commercial application for RMBs. Generally, a Mg metal anode can rapidly react with trace water (even below than 20 ppm) and form undesired passivation layers, leading to irreversible Mg plating/stripping behaviors.[63] Herein, we carried out this measurement by adding 10 000 ppm of H_2O to four electrolytes, respectively. Interestingly, for S2 solvent, it can still retain remarkable electrochemical performance (low overpotential of about 0.05 V and high CE over 80%) with the addition of 10 000 ppm of H_2O (Figure 4a−c). And even with the addition of 20 000 ppm of H_2O, the situation for S2 solvent is almost the same (Figure S15a−c). The CV curves of S2 solvent with the addition of 10 000 and 20 000 ppm of H_2O can also show reversible plating/stripping behaviors (Figure S16a,b). And the XPS measurement of the components of cycled Mg in S2 solvent with the addition of 10 000 ppm of H_2O shows a similar result as before (Figure S17a,b). Besides, the phenomenon happens in S1 and S3 solvents as well (Figure S18d−i). However, for DME solvent, the electrochemical performance cannot be maintained and becomes bad sharply (Figure S18a−c). It indicates the Mg deposition/stripping processes in S1, S2, or S3 solvent containing amino groups is less affected by water than that in DME, suggesting the activities of water molecules of these electrolytes are different. To explore the cause of this obvious electrochemical performance difference, the DME system and S2 system are chosen as two study representatives. Quantum chemical calculations show that the binding energies of hydrogen bonds for dimers $H_2O\cdots H_2O$, $H_2O\cdots$DME, and $H_2O\cdots$S2 are −19.0, −21.3, and −29.1 kJ/mol, respectively (Figure 4d), and the vibration wavenumbers of the three hydrogen bonds are 3487, 3484, and 3238 cm^{-1}, respectively (shown in the inset in Figure 4e). The higher binding energy and lower vibration wavenumber both indicate the combining ability of an amino group ($-NH_2$) to H_2O is higher compared with the hydroxyl group (−OH) and ether group (−O−). This is also confirmed by the classical dynamics simulation result. As shown in Figure S19a,b, the coordination number of H_2O to N atom is 2.1, while that to an O atom is only 0.4, indicating water molecules tend to form a hydrogen bond with an amino group ($-NH_2$).

This explanation is further demonstrated by the Fourier transform infrared (FT-IR) spectroscopy (Figure 4e). An obvious characteristic peak at about 3400 cm^{-1} is observed after the addition of water in the electrolyte with DME solvent, indicating the existence of free H_2O molecules rather than constrained H_2O molecules. In sharp contrast, after the addition of water in S2 solvent, the FT-IR spectroscopy results do not show significant differences except the increase of peak intensity at about 3200 cm^{-1}, which indicates H_2O molecules are almost combined with S2 solvent molecules via strong hydrogen bonds, showing nearly no free H_2O molecules in the electrolyte. The ^{19}F NMR spectroscopy results are in perfect agreement with FT-IR data as expected (Figure S20). In DME solvent, chemical shifts show an apparent change in two electrolytes with H_2O and without H_2O, demonstrating most H_2O molecules are not constrained and still can interact with $TFSI^-$ anion; while in S2 solvent, this change of chemical shifts becomes inconspicuous, which indirectly indicates H_2O is not free, so this hardly affects the $TFSI^-$ anion. The influence of water to a solvated structure is investigated as well. As shown in Figure 4f, the binding free energies of water with a solvated Mg ion in DME and S2 are −30.2 and 18.0 kJ/mol respectively, and this indicates the entry of water molecules into the first solvated layer of Mg^{2+} ion is spontaneous in DME solution and not spontaneous in S2, showing the Mg^{2+} solvated structure in S2 can still remain even after the addition of water. Besides, we also investigate the difference of the H_2 evolution rate in DME and S2 electrolytes, and the H_2O content was increased to 100 000 ppm to make the experimental phenomenon more obvious under macroscopic observation. For DME solvent, macroscopic gas generation is observed after Mg foils immerse into the electrolyte (Video S1); while for S2

https://doi.org/10.1021/acsenergylett.2c02525
ACS Energy Lett. 2023, 8, 780−789

solvent, the Mg foils still remain stable as before (Video S2). This visualization measurement can further confirm the activity of H_2O is suppressed obviously in S2 solvent compared with DME solvent.

As a result, in ether solvents (such DME, Figure 4g), the H_2O molecules are less constrained by hydrogen bonds and more likely to coordinate with Mg^{2+} or attach to the surface of Mg metal, which can easily allow hydrogen evolution and formation of passivation layers during the Mg plating/stripping process. While for the amine solvents (such as S2, Figure 4h), most H_2O molecules are constrained by strong hydrogen bonds with $-NH_2$, leading to the retained Mg^{2+} solvated structure and nearly no active H_2O molecules in the electrolyte under macroscopic scale. Thus, the fast interfacial kinetics can remain, and the surface of Mg metal is still fresh even after the addition of water, which can support a reversible Mg plating/stripping process as before. This interesting discovery can provide a totally new method to enhance the water-resistant ability of electrolyte, which is by the strong interaction between solvent molecule and water to restrain the activity of H_2O molecules.

The practical operation situation of a full cell is investigated as well. A classical Chevrel phase Mo_6S_8 material is used as the cathode (owing to the linear-sweep voltammetry measurement results, Figure S21a−d) to evaluate the electrochemical performance of the Mg//Mo_6S_8 full cell with an electrolyte of the best S2 solvent. As shown in Figure S22a,b, the full cell with S2 solvent can run stably for over 100 cycles and deliver a specific capacity of about 70 mAh g^{-1} in the 100th cycle, indicating the outstanding compatibility of S2 solvent for both the anode and cathode. Additionally, the generality of the S2 solvent is demonstrated as well, such as a higher salt concentration (Figure S23a−d) and mixing with other ether solvent as the additive (Figures S24a,b and S25a−c), indicating the great potential of amine solvents for the further study.

In summary, we elaborately design a series of solvent molecules according to the structure of DME and find out the S2 (3-methoxypropylamine) can be used as an effective new solvent to achieve superior electrochemical performance with low overpotential (below than 0.05 V) and high average CE (over 95.9%) for over 350 cycles. To further understand the relationship between electrochemical performances and solvated structure, the interface reaction process of the Mg metal anode is investigated by spectroscopic characterization and theoretical calculation. We divide the reaction of interface electrochemistry into two elementary processes, namely, the Marcus charge transfer process and desolvation process, and discover the energy barriers of these two processes are antagonistic and extremely influenced by coordination ability of solvent molecules. The S2 solvent exactly possesses low energy barriers of these two processes at the same time and exhibits an excellent interfacial kinetics process in consequent. In addition, S2 solvent possesses a remarkable water-resistant property and retains its excellent electrochemical performances even with the addition of over 10 000 ppm of H_2O, which is attributed to strong hydrogen bonds between amine groups and water, leading to the retained Mg^{2+} solvated structure and nearly no active H_2O molecules in the electrolyte. This report reveals the crucial influences of solvent molecule structures as well as their coordination abilities in the interface electrochemical reaction of a Mg metal anode and proposes a universal design principle of solvent molecules for the first time in RMBs.

■ ASSOCIATED CONTENT

Supporting Information

The Supporting Information is available free of charge at https://pubs.acs.org/doi/10.1021/acsenergylett.2c02525.

Experimental section; calculation methods; supplementary figures and tables (PDF)

Video S1: For DME solvent, macroscopic gas generation is observed after Mg foils are immersed into the electrolyte (MP4)

Video S2: For S2 solvent, the Mg foils still remain stable as before (MP4)

■ AUTHOR INFORMATION

Corresponding Authors

Jing Zeng − *College of Chemistry and Chemical Engineering, Xiamen University, Xiamen 361005, PR China; State-Province Joint Engineering Laboratory of Power Source Technology for New Energy Vehicle, State Key Laboratory of Physical Chemistry of Solid Surfaces, Engineering Research Center of Electrochemical Technology, Ministry of Education, Collaborative Innovation Center of Chemistry for Energy Materials, Xiamen University, Xiamen 361005, PR China*; Email: zengjing@xmu.edu.cn

Jinbao Zhao − *College of Chemistry and Chemical Engineering, Xiamen University, Xiamen 361005, PR China; State-Province Joint Engineering Laboratory of Power Source Technology for New Energy Vehicle, State Key Laboratory of Physical Chemistry of Solid Surfaces, Engineering Research Center of Electrochemical Technology, Ministry of Education, Collaborative Innovation Center of Chemistry for Energy Materials, Xiamen University, Xiamen 361005, PR China*; orcid.org/0000-0002-2753-7508; Email: jbzhao@xmu.edu.cn

Authors

Fei Wang − *College of Chemistry and Chemical Engineering, Xiamen University, Xiamen 361005, PR China; State-Province Joint Engineering Laboratory of Power Source Technology for New Energy Vehicle, State Key Laboratory of Physical Chemistry of Solid Surfaces, Engineering Research Center of Electrochemical Technology, Ministry of Education, Collaborative Innovation Center of Chemistry for Energy Materials, Xiamen University, Xiamen 361005, PR China*

Haiming Hua − *College of Chemistry and Chemical Engineering, Xiamen University, Xiamen 361005, PR China; State-Province Joint Engineering Laboratory of Power Source Technology for New Energy Vehicle, State Key Laboratory of Physical Chemistry of Solid Surfaces, Engineering Research Center of Electrochemical Technology, Ministry of Education, Collaborative Innovation Center of Chemistry for Energy Materials, Xiamen University, Xiamen 361005, PR China*

Dongzheng Wu − *College of Chemistry and Chemical Engineering, Xiamen University, Xiamen 361005, PR China; State-Province Joint Engineering Laboratory of Power Source Technology for New Energy Vehicle, State Key Laboratory of Physical Chemistry of Solid Surfaces, Engineering Research Center of Electrochemical Technology, Ministry of Education, Collaborative Innovation Center of Chemistry for Energy Materials, Xiamen University, Xiamen 361005, PR China*

Jialin Li − *College of Chemistry and Chemical Engineering, Xiamen University, Xiamen 361005, PR China; State-Province Joint Engineering Laboratory of Power Source*

https://doi.org/10.1021/acsenergylett.2c02525
ACS Energy Lett. 2023, 8, 780−789

Technology for New Energy Vehicle, State Key Laboratory of Physical Chemistry of Solid Surfaces, Engineering Research Center of Electrochemical Technology, Ministry of Education, Collaborative Innovation Center of Chemistry for Energy Materials, Xiamen University, Xiamen 361005, PR China

Yaoqi Xu − *College of Chemistry and Chemical Engineering, Xiamen University, Xiamen 361005, PR China; State-Province Joint Engineering Laboratory of Power Source Technology for New Energy Vehicle, State Key Laboratory of Physical Chemistry of Solid Surfaces, Engineering Research Center of Electrochemical Technology, Ministry of Education, Collaborative Innovation Center of Chemistry for Energy Materials, Xiamen University, Xiamen 361005, PR China*

Xianzhen Nie − *College of Chemistry and Chemical Engineering, Xiamen University, Xiamen 361005, PR China; State-Province Joint Engineering Laboratory of Power Source Technology for New Energy Vehicle, State Key Laboratory of Physical Chemistry of Solid Surfaces, Engineering Research Center of Electrochemical Technology, Ministry of Education, Collaborative Innovation Center of Chemistry for Energy Materials, Xiamen University, Xiamen 361005, PR China*

Yichao Zhuang − *College of Chemistry and Chemical Engineering, Xiamen University, Xiamen 361005, PR China; State-Province Joint Engineering Laboratory of Power Source Technology for New Energy Vehicle, State Key Laboratory of Physical Chemistry of Solid Surfaces, Engineering Research Center of Electrochemical Technology, Ministry of Education, Collaborative Innovation Center of Chemistry for Energy Materials, Xiamen University, Xiamen 361005, PR China*

Complete contact information is available at: https://pubs.acs.org/10.1021/acsenergylett.2c02525

Author Contributions

F.W. and H.H. contributed equally to this work.

Notes

The authors declare no competing financial interest.

■ ACKNOWLEDGMENTS

The authors gratefully acknowledge the National Natural Science Foundation of China (Nos. 21875198, 22005257, and 22021001), the Natural Science Foundation of Fujian Province of China (No. 2020J05009), and NFFTBS No. J1310024 for financial support. We are grateful to Dr. Yuhao Hong at Tan Kah Kee Innovation Laboratory (IKKEM), Center for Micronano Fabrication and Advanced Characterization, Xiamen University, for help with the XPS measurement. The authors acknowledge Beijng PARATERA Tech CO., Ltd. for providing HPC resources that have contributed to the research results reported within this paper. URL: https://paratera.com/ .

■ REFERENCES

(1) Goodenough, J. B.; Park, K.-S. The Li-Ion Rechargeable Battery: A Perspective. *J. Am. Chem. Soc.* **2013**, *135* (4), 1167−1176.

(2) Fan, E. S.; Li, L.; Wang, Z. P.; Lin, J.; Huang, Y. X.; Yao, Y.; Chen, R. J.; Wu, F. Sustainable Recycling Technology for Li-Ion Batteries and Beyond: Challenges and Future Prospects. *Chem. Rev.* **2020**, *120* (14), 7020−7063.

(3) Zhang, X.; Yang, Y. A.; Zhou, Z. Towards practical lithium-metal anodes. *Chem. Soc. Rev.* **2020**, *49* (10), 3040−3071.

(4) Goodenough, J. B.; Kim, Y. Challenges for Rechargeable Li Batteries. *Chem. Mater.* **2010**, *22* (3), 587−603.

(5) Etacheri, V.; Marom, R.; Elazari, R.; Salitra, G.; Aurbach, D. Challenges in the development of advanced Li-ion batteries-a review. *Energy Environ. Sci.* **2011**, *4* (9), 3243−3262.

(6) Xu, K. Electrolytes and Interphases in Li-Ion Batteries and Beyond. *Chem. Rev.* **2014**, *114* (23), 11503−11618.

(7) Zhang, J. G.; Xu, W.; Xiao, J.; Cao, X.; Liu, J. Lithium Metal Anodes with Nonaqueous Electrolytes. *Chem. Rev.* **2020**, *120* (24), 13312−13348.

(8) Lv, R. J.; Guan, X. Z.; Zhang, J. H.; Xia, Y. Y.; Luo, J. Y. Enabling Mg metal anodes rechargeable in conventional electrolytes by fast ionic transport interphase. *Natl. Sci. Rev.* **2020**, *7* (2), 333−341.

(9) Bae, J.; Park, H.; Guo, X.; Zhang, X.; Warner, J. H.; Yu, G. High-performance magnesium metal batteries via switching the passivation film into a solid electrolyte interphase. *Energy Environ. Sci.* **2021**, *14* (8), 4391−4399.

(10) Tian, Y.; Zeng, G.; Rutt, A.; Shi, T.; Kim, H.; Wang, J.; Koettgen, J.; Sun, Y.; Ouyang, B.; Chen, T.; Lun, Z.; Rong, Z.; Persson, K.; Ceder, G. Promises and Challenges of Next-Generation "Beyond Li-ion" Batteries for Electric Vehicles and Grid Decarbonization. *Chem. Rev.* **2021**, *121* (3), 1623−1669.

(11) Liang, Y. L.; Dong, H.; Aurbach, D.; Yao, Y. Current status and future directions of multivalent metal-ion batteries. *Nat. Energy* **2020**, *5* (9), 646−656.

(12) Wang, L.; Welborn, S. S.; Kumar, H.; Li, M.; Wang, Z.; Shenoy, V. B.; Detsi, E. High-Rate and Long Cycle-Life Alloy-Type Magnesium-Ion Battery Anode Enabled Through (De)-magnesiation-Induced Near-Room-Temperature Solid−Liquid Phase Transformation. *Adv. Energy Mater.* **2019**, *9* (45), 1902086.

(13) Liu, J.; Zhang, J. L.; Zhang, Z. H.; Du, A. B.; Dong, S. M.; Zhou, Z. F.; Guo, X. S.; Wang, Q. F.; Li, Z. J.; Li, G. C.; Cui, G. L. Epitaxial Electrocrystallization of Magnesium via Synergy of Magnesiophilic Interface, Lattice Matching, and Electrostatic Confinement. *ACS Nano* **2022**, *16* (6), 9894−9907.

(14) Wang, F.; Wu, D. Z.; Zhuang, Y. C.; Li, J. L.; Nie, X. Z.; Zeng, J.; Zhao, J. B. Modification of a Cu Mesh with Nanowires and Magnesiophilic Ag Sites to Induce Uniform Magnesium Deposition. *ACS Appl. Mater. Interfaces* **2022**, *14* (27), 31148−31159.

(15) Liu, F. F.; Wang, T. T.; Liu, X. B.; Fan, L. Z. Challenges and Recent Progress on Key Materials for Rechargeable Magnesium Batteries. *Adv. Energy Mater.* **2021**, *11* (2), 2000787.

(16) Zhang, J.; Chang, Z.; Zhang, Z.; Du, A.; Dong, S.; Li, Z.; Li, G.; Cui, G. Current Design Strategies for Rechargeable Magnesium-Based Batteries. *ACS Nano* **2021**, *15* (10), 15594−15624.

(17) Son, S. B.; Gao, T.; Harvey, S. P.; Steirer, K. X.; Stokes, A.; Norman, A.; Wang, C. S.; Cresce, A.; Xu, K.; Ban, C. M. An artificial interphase enables reversible magnesium chemistry in carbonate electrolytes. *Nat. Chem.* **2018**, *10* (5), 532−539.

(18) Zhao, Y. M.; Du, A. B.; Dong, S. M.; Jiang, F.; Guo, Z. Y.; Ge, X. S.; Qu, X. L.; Zhou, X. H.; Cui, G. L. A Bismuth-Based Protective Layer for Magnesium Metal Anode in Noncorrosive Electrolytes. *ACS Energy Lett.* **2021**, *6* (7), 2594−2601.

(19) Wu, D.; Wang, F.; Yang, H.; Xu, Y.; Zhuang, Y.; Zeng, J.; Yang, Y.; Zhao, J. Realizing rapid electrochemical kinetics of Mg2+ in Ti-Nb oxides through a Li+ intercalation activated strategy toward extremely fast charge/discharge dual-ion batteries. *Energy Storage Mater.* **2022**, *52*, 94−103.

(20) Muldoon, J.; Bucur, C. B.; Gregory, T. Fervent Hype behind Magnesium Batteries: An Open Call to Synthetic Chemists-Electrolytes and Cathodes Needed. *Angew. Chem.-Int. Ed.* **2017**, *56* (40), 12064−12084.

(21) Mohtadi, R.; Mizuno, F. Magnesium batteries: Current state of the art, issues and future perspectives. *Beilstein J. Nanotechnol.* **2014**, *5*, 1291−1311.

(22) Mohtadi, R.; Tutusaus, O.; Arthur, T. S.; Zhao-Karger, Z.; Fichtner, M. The metamorphosis of rechargeable magnesium batteries. *Joule* **2021**, *5* (3), 581−617.

(23) Zhang, Y.; Li, J.; Zhao, W.; Dou, H.; Zhao, X.; Liu, Y.; Zhang, B.; Yang, X. Defect-Free Metal-Organic Framework Membrane for

Precise Ion/Solvent Separation toward Highly Stable Magnesium Metal Anode. *Adv. Mater.* **2022**, *34*, No. 2108114.
(24) Li, X. G.; Gao, T.; Han, F. D.; Ma, Z. H.; Fan, X. L.; Hou, S.; Eidson, N.; Li, W. S.; Wang, C. S. Reducing Mg Anode Overpotential via Ion Conductive Surface Layer Formation by Iodine Additive. *Adv. Energy Mater.* **2018**, *8* (7), 1802041.
(25) Yoo, H. D.; Shterenberg, I.; Gofer, Y.; Gershinsky, G.; Pour, N.; Aurbach, D. Mg rechargeable batteries: an on-going challenge. *Energy Environ. Sci.* **2013**, *6* (8), 2265−2279.
(26) Muldoon, J.; Bucur, C. B.; Gregory, T. Quest for Nonaqueous Multivalent Secondary Batteries: Magnesium and Beyond. *Chem. Rev.* **2014**, *114* (23), 11683−11720.
(27) Guo, Z.; Zhao, S.; Li, T.; Su, D.; Guo, S.; Wang, G. Recent Advances in Rechargeable Magnesium-Based Batteries for High-Efficiency Energy Storage. *Adv. Energy Mater.* **2020**, *10* (21), 1903591.
(28) Wang, C. Y.; Huang, Y.; Lu, Y. H.; Pan, H. G.; Xu, B. B.; Sun, W. P.; Yan, M.; Jiang, Y. Z. Reversible Magnesium Metal Anode Enabled by Cooperative Solvation/Surface Engineering in Carbonate Electrolytes. *Nano-Micro Letters* **2021**, *13* (1), 195.
(29) Xiao, J. H.; Zhang, X. X.; Fan, H. Y.; Zhao, Y. X.; Su, Y.; Liu, H. W.; Li, X. Z.; Su, Y. P.; Yuan, H.; Pan, T.; Lin, Q. Y.; Pan, L. D.; Zhang, Y. G. Stable Solid Electrolyte Interphase In Situ Formed on Magnesium-Metal Anode by using a Perfluorinated Alkoxide-Based All-Magnesium Salt Electrolyte. *Adv. Mater.* **2022**, *34* (30), 2203783.
(30) Zhu, J.-J.; Wang, F.-F.; Guo, Y.-S.; Yang, J.; Nuli, Y.-N.; Wang, J.-L. Application of Ionic Liquid PP14 TFSI in Electrolyte Systems for Rechargeable Mg Batteries. *J. Electrochem* **2014**, *20*, 128−133.
(31) Liang, Z.; Ban, C. Strategies to Enable Reversible Magnesium Electrochemistry: From Electrolytes to Artificial Solid-Electrolyte Interphases. *Angew. Chem.-Int. Ed.* **2021**, *60* (20), 11036−11047.
(32) Shi, J. Y.; Zhang, J.; Guo, J. C.; Lu, J. Interfaces in rechargeable magnesium batteries. *Nanoscale Horiz.* **2020**, *5* (11), 1467−1475.
(33) Tutusaus, O.; Mohtadi, R.; Arthur, T. S.; Mizuno, F.; Nelson, E. G.; Sevryugina, Y. V. An Efficient Halogen-Free Electrolyte for Use in Rechargeable Magnesium Batteries. *Angew. Chem.-Int. Ed.* **2015**, *54* (27), 7900−7904.
(34) Muldoon, J.; Bucur, C. B.; Oliver, A. G.; Sugimoto, T.; Matsui, M.; Kim, H. S.; Allred, G. D.; Zajicek, J.; Kotani, Y. Electrolyte roadblocks to a magnesium rechargeable battery. *Energy Environ. Sci.* **2012**, *5* (3), 5941−5950.
(35) Song, J.; Sahadeo, E.; Noked, M.; Lee, S. B. Mapping the Challenges of Magnesium Battery. *J. Phys. Chem. Lett.* **2016**, *7* (9), 1736−1749.
(36) Zhang, Z. H.; Cui, Z. L.; Qiao, L. X.; Guan, J.; Xu, H. M.; Wang, X. G.; Hu, P.; Du, H. P.; Li, S. Z.; Zhou, X. H.; Dong, S. M.; Liu, Z. H.; Cui, G. L.; Chen, L. Q. Novel Design Concepts of Efficient Mg-Ion Electrolytes toward High-Performance Magnesium-Selenium and Magnesium-Sulfur Batteries. *Adv. Energy Mater.* **2017**, *7* (11), 1602055.
(37) Deivanayagam, R.; Ingram, B. J.; Shahbazian-Yassar, R. Progress in development of electrolytes for magnesium batteries. *Energy Storage Mater.* **2019**, *21*, 136−153.
(38) Shuai, H.; Xu, J.; Huang, K. Progress in retrospect of electrolytes for secondary magnesium batteries. *Coord. Chem. Rev.* **2020**, *422*, 213478.
(39) Attias, R.; Salama, M.; Hirsch, B.; Goffer, Y.; Aurbach, D. Anode-Electrolyte Interfaces in Secondary Magnesium Batteries. *Joule* **2019**, *3* (1), 27−52.
(40) Pei, C.; Xiong, F.; Yin, Y.; Liu, Z.; Tang, H.; Sun, R.; An, Q.; Mai, L. Recent Progress and Challenges in the Optimization of Electrode Materials for Rechargeable Magnesium Batteries. *Small* **2021**, *17*, 2004108.
(41) Carter, T. J.; Mohtadi, R.; Arthur, T. S.; Mizuno, F.; Zhang, R.; Shirai, S.; Kampf, J. W. Boron clusters as highly stable magnesium-battery electrolytes. *Angew. Chem.-Int. Ed.* **2014**, *53* (12), 3173−7.
(42) Mizrahi, O.; Amir, N.; Pollak, E.; Chusid, O.; Marks, V.; Gottlieb, H.; Larush, L.; Zinigrad, E.; Aurbach, D. Electrolyte solutions with a wide electrochemical window for recharge magnesium batteries. *J. Electrochem. Soc.* **2008**, *155* (2), A103−A109.
(43) Doe, R. E.; Han, R.; Hwang, J.; Gmitter, A. J.; Shterenberg, I.; Yoo, H. D.; Pour, N.; Aurbach, D. Novel, electrolyte solutions comprising fully inorganic salts with high anodic stability for rechargeable magnesium batteries. *Chem. Commun.* **2014**, *50* (2), 243−245.
(44) Du, A. B.; Zhang, Z. H.; Qu, H. T.; Cui, Z. L.; Qiao, L. X.; Wang, L. L.; Chai, J. C.; Lu, T.; Dong, S. M.; Dong, T. T.; Xu, H. M.; Zhou, X. H.; Cui, G. L. An efficient organic magnesium borate-based electrolyte with non-nucleophilic characteristics for magnesium-sulfur battery. *Energy Environ. Sci.* **2017**, *10* (12), 2616−2625.
(45) Kim, S. S.; Bevilacqua, S. C.; See, K. A. Conditioning-Free Mg Electrolyte by the Minor Addition of Mg(HMDS)(2). *ACS Appl. Mater. Interfaces* **2020**, *12* (5), 5226−5233.
(46) Wang, P. W.; Trueck, J.; Hacker, J.; Schlosser, A.; Kuester, K.; Starke, U.; Reinders, L.; Buchmeiser, M. R. A design concept for halogen-free Mg2+/Li+-dual salt-containing gel-polymer-electrolytes for rechargeable magnesium batteries. *Energy Storage Mater.* **2022**, *49*, 509−517.
(47) Wang, L. P.; Li, Z. Y.; Meng, Z.; Xiu, Y. L.; Dasari, B.; Zhao-Karger, Z.; Fichtner, M. Designing gel polymer electrolyte with synergetic properties for rechargeable magnesium batteries. *Energy Storage Mater.* **2022**, *48*, 155−163.
(48) Wang, J. H.; Zhao, W. Y.; Dou, H. L.; Wan, B. X.; Zhang, Y. J.; Li, W. F.; Zhao, X. L.; Yang, X. W. Electrostatic Shielding Guides Lateral Deposition for Stable Interphase toward Reversible Magnesium Metal Anodes. *ACS Appl. Mater. Interfaces* **2020**, *12* (17), 19601−19606.
(49) Li, Y.; Zuo, P.; Zhang, N.; Yin, X.; Li, R.; He, M.; Huo, H.; Ma, Y.; Du, C.; Gao, Y.; Yin, G. Improving electrochemical performance of rechargeable magnesium batteries with conditioning-free Mg-Cl complex electrolyte. *Chem. Eng. J.* **2021**, *403*, 126398.
(50) Pavcnik, T.; Lozinsek, M.; Pirnat, K.; Vizintin, A.; Mandai, T.; Aurbach, D.; Dominko, R.; Bitenc, J. On the Practical Applications of the Magnesium Fluorinated Alkoxyaluminate Electrolyte in Mg Battery Cells. *ACS Appl. Mater. Interfaces* **2022**, *14* (23), 26766−26774.
(51) Hou, S.; Ji, X.; Gaskell, K.; Wang, P.-F.; Wang, L.; Xu, J.; Sun, R.; Borodin, O.; Wang, C. Solvation sheath reorganization enables divalent metal batteries with fast interfacial charge transfer kinetics. *Science* **2021**, *374* (6564), 172−178.
(52) Zhao, W. Y.; Pan, Z. H.; Zhang, Y. J.; Liu, Y.; Dou, H. L.; Shi, Y. Y.; Zuo, Z. J.; Zhang, B. W.; Chen, J. P.; Zhao, X. L.; Yang, X. W. Tailoring Coordination in Conventional Ether-Based Electrolytes for Reversible Magnesium-Metal Anodes. *Angew. Chem.-Int. Ed.* **2022**, *61* (30), e202205187.
(53) Lin, S. S.; Hua, H. M.; Lai, P. B.; Zhao, J. B. A Multifunctional Dual-Salt Localized High-Concentration Electrolyte for Fast Dynamic High-Voltage Lithium Battery in Wide Temperature Range. *Adv. Energy Mater.* **2021**, *11* (36), 2101775.
(54) Thenuwara, A. C.; Shetty, P. P.; Kondekar, N.; Sandoval, S. E.; Cavallaro, K.; May, R.; Yang, C. T.; Marbella, L. E.; Qi, Y.; McDowell, M. T. Efficient Low-Temperature Cycling of Lithium Metal Anodes by Tailoring the Solid-Electrolyte Interphase. *ACS Energy Lett.* **2020**, *5* (7), 2411−2420.
(55) Jackle, M.; Helmbrecht, K.; Smits, M.; Stottmeister, D.; Gross, A. Self-diffusion barriers: possible descriptors for dendrite growth in batteries? *Energy Environ. Sci.* **2018**, *11* (12), 3400−3407.
(56) Marcus, R. A. ELECTRON-TRANSFER REACTIONS IN CHEMISTRY - THEORY AND EXPERIMENT (NOBEL LECTURE). *Angew. Chem.-Int. Ed. Engl.* **1993**, *32* (8), 1111−1121.
(57) Nelsen, S. F.; Blackstock, S. C.; Kim, Y. ESTIMATION OF INNER SHELL MARCUS TERMS FOR AMINO NITROGEN-COMPOUNDS BY MOLECULAR-ORBITAL CALCULATIONS. *J. Am. Chem. Soc.* **1987**, *109* (3), 677−682.
(58) Kopač Lautar, A.; Bitenc, J.; Rejec, T.; Dominko, R.; Filhol, J. S.; Doublet, M. L. Electrolyte Reactivity in the Double Layer in Mg

Batteries: An Interface Potential-Dependent DFT Study. *J. Am. Chem. Soc.* **2020**, *142* (11), 5146−5153.
(59) Chen, X.; Hou, T. Z.; Li, B.; Yan, C.; Zhu, L.; Guan, C.; Cheng, X. B.; Peng, H. J.; Huang, J. Q.; Zhang, Q. Towards stable lithium-sulfur batteries: Mechanistic insights into electrolyte decomposition on lithium metal anode. *Energy Storage Mater.* **2017**, *8*, 194−201.
(60) Lu, T.; Chen, F. W. Multiwfn: A multifunctional wavefunction analyzer. *J. Comput. Chem.* **2012**, *33* (5), 580−592.
(61) Lu, T.; Chen, F. W. Quantitative analysis of molecular surface based on improved Marching Tetrahedra algorithm. *J. Mol. Graph.* **2012**, *38*, 314−323.
(62) Murray, J. S.; Politzer, P. The electrostatic potential: an overview. *Wiley Interdiscip. Rev.-Comput. Mol. Sci.* **2011**, *1* (2), 153−163.
(63) He, S. J.; Luo, J.; Liu, T. L. MgCl2/AlCl3 electrolytes for reversible Mg deposition/stripping: electrochemical conditioning or not? *J. Mater. Chem. A* **2017**, *5* (25), 12718−12722.

https://doi.org/10.1021/acsenergylett.2c02525
ACS Energy Lett. 2023, 8, 780−789